

GAMMA-RAY FLARES AND VLBI OUTBURSTS OF BLAZARS

M.M. ROMANOVA

Space Research Institute, Russian Academy of Sciences, Moscow, Russia; and
 Department of Astronomy, Cornell University, Ithaca, NY 14853-6801; romanova@astrosun.tn.cornell.edu

R.V.E. LOVELACE

Department of Astronomy, Cornell University, Ithaca, NY 14853-6801; rvl1@cornell.edu
Draft version February 5, 2008

ABSTRACT

A model is developed for the time dependent electromagnetic - radio to gamma-ray - emission of active galactic nuclei, specifically, the blazars, based on the acceleration and creation of leptons at a propagating discontinuity or *front* of a self-collimated Poynting flux jet. The front corresponds to a discrete relativistic jet component as observed with very-long-baseline-interferometry (VLBI). Equations are derived for the number, momentum, and energy of particles in the front taking into account synchrotron, synchrotron-self-Compton (SSC), and inverse-Compton processes as well as photon-photon pair production. The apparent synchrotron, SSC, and inverse Compton luminosities as functions of time are determined. Predictions of the model are compared with observations in the gamma, optical, and radio bands. The delay between the high-energy gamma-ray flare and the onset of the radio is explained by self-absorption and/or free-free absorption by external plasma. Two types of gamma-ray flares are predicted, Compton dominated or SSC dominated, depending on the initial parameters in the front. The theory is applied to the recently observed gamma-ray flare of the blazar PKS 1622-297 (Mattox et al. 1996). Approximate agreement of theoretical and observed light curves is obtained for a viewing angle $\theta_{obs} \sim 0.1$ rad, a black hole mass $M \sim 3 \times 10^9 M_{\odot}$, and a magnetic field at the base of the jet $B_o \sim 10^3$ G.

Subject headings: active—galaxies: quasars—galaxies: jets—galaxies: gamma-rays—galaxies

1. INTRODUCTION

New understanding of the nature of Active Galactic Nuclei (AGNs) has come from the discovery of the high energy gamma-ray radiation in the range $50 - 10^4$ MeV by the EGRET instrument on the Compton gamma-ray Observatory (e.g., Hartman et al. 1992; Mattox et al. 1993; Thompson et al. 1993). This radiation is observed from a sub-class of AGNs termed blazars, which include Optically Violently Variable (OVV) quasars and BL Lac objects and which show strong variability in all wavebands from radio to gamma. Many of the objects reveal ‘super-luminal’ jets in VLBI maps which indicate that we observe matter of the jet pointed nearly towards us and that the jet matter moves with relativistic speed.

Prior to the Compton Observatory measurements, prediction of strong, collimated gamma-ray emission from AGN relativistic jet sources was made by the electromagnetic cascade model of Lovelace, MacAuslan, and Burns (1979) and Burns and Lovelace (1982). More recently, a number of theoretical models have been developed to explain the observed gamma-ray emission of AGNs (see review by Sikora 1994). In most of the models the gamma-ray radiation is ascribed to inverse-Compton scattering of relativistic electrons and possibly positrons (Lorentz factors $\gamma \sim 10^2 - 10^3$) of a jet having relativistic bulk motion (Lorentz factor $\Gamma \sim 10$) with soft photons (energies $\sim 1 - 10^2$ eV). The soft photons can arise from the synchrotron emission of the relativistic electrons in the jet as in the synchrotron-self-Compton (SSC) models (Maraschi, Ghisellini, and Celotti 1992; Marscher and Bloom, 1992) or from the direct or scattered thermal ra-

diation from an accretion disk (Dermer, Schlickeiser, and Mastichiadis 1992; Blandford 1993; and Sikora, Begelman, and Rees 1994), or from a single cloud (Ghisellini and Madau 1996). The spectrum of blazars in a pair cascade model was calculated by Levinson and Blandford (1995) and Levinson (1996). In different models, ultra high energy protons (Lorentz factors $> 10^6$) are postulated to cause a cascade, the product particles of which produce the observed radiation (Mannheim and Biermann 1992), or the jets considered to be ultra relativistic with bulk Lorentz factors $\Gamma > 10^4$ (Coppi, Kartje, and Königl 1993).

Here, we propose that the main driving force for the observed superluminal jet components is a finite amplitude discontinuity in a Poynting flux jet. A brief discussion of the model was given earlier (Lovelace and Romanova 1996). A rapid change in the Poynting jet outflow from a disk can result from implosive accretion in a disk with an ordered magnetic field (Lovelace, Romanova, and Newman 1994). Propagation of newly expelled EM field and matter from the disk with higher velocity than the old jet can under certain conditions lead to the formation of a pair of shock waves as in the case of non-relativistic hydrodynamic flow (Raga et al. 1990). Particle acceleration in the front may result from the shocks or from annihilation and/or reconnection of oppositely directed magnetic fields in the front (Romanova and Lovelace 1992 and Lovelace, Newman, and Romanova 1996).

Section 2 derives a complete set of equations for the front, specifically, equations for the total number of particles, the total momentum, energy, and magnetic flux in the front. Section 3 discusses and summarizes the be-

havior of the solutions of the front equations. Section 4 gives comparisons of predictions of the theory with observations. Conclusions of this work are given in Section 5.

2. THEORY

We use an inertial, cylindrical coordinate system (r, ϕ, z) with the origin at the black hole's center and the z -axis normal to the accretion disk as shown in Figure 1. This is referred to as the 'lab frame'. We consider that Poynting flux jets propagate symmetrically away from the disk in the $\pm z$ directions, but focus our attention on the approaching $+z$ jet. A Poynting flux jet is *self-collimated*, with energy, momentum, and angular momentum transported mainly by the electromagnetic fields (Lovelace, Wang, and Sulkanen 1987). The collimation results from the toroidal magnetic field at the edge of the jet. A steady Poynting jet can be characterized in the lab frame by its asymptotic ($z \gg r_o$) magnetic field $B_\phi = -B[r_o/r_j(z)]$, and electric field $E_r = -(v/c)B[r_o/r_j(z)]$ at the jet's edge, $r = r_j(z)$, where r_o is the jet's radius at $z = 0$, $v = \text{const.}$ is the jet's axial velocity, and B is the lab frame field strength at $z = 0$.

The jet plasma consists of both ions and leptons (electrons and positrons) with the ratio of leptons to ions f_{li} . The initial jet radius is taken to be $r_o = 6GM/c^2$, where M is the black hole mass. The energy flux (luminosity) of the $+z$ jet is the Poynting flux $L_j = vB^2r_o^2/8 = \text{constant}$.

We propose that the Poynting jet from the disk changes abruptly at time $t = 0$. That is, the jet parameters change from values with subscript (1) to subscript (2) at $t = 0$, ($B_1, n_{i1}, v_1, f_{li1}$) \rightarrow ($B_2, n_{i2}, v_2, f_{li2}$). In actuality the change will be with a time scale determined by the disk dynamics as in the implosive accretion model of Lovelace et al. (1994). This time scale may be as short as r_o/c in the lab frame. In the present work we consider $b \equiv B_1/B_2 < 1$, $\nu \equiv n_{i1}/n_{i2}$, $v_1 < v_2$, $f_{li1} = f_{li2}$, where n_i is the number density of ions. The change in the jet parameters produces a 'front' which propagates outward as indicated in Figure 1. The front may involve a pair of shock waves, one for the incoming old jet matter and the other for the incoming new jet matter. We let $Z(t) = z(t)/r_o$ denote the dimensionless axial distance of the front. We also use lab time $T = t/(r_o/c)$, speed of the front $U(T) = dZ/dT = (dz/dt)/c$, and bulk Lorentz factor $\Gamma = (1 - U^2)^{-1/2}$. We let $V_{1,2} = v_{1,2}/c$ and $\Gamma_{1,2} = (1 - V_{1,2}^2)^{-1/2}$. The time measured in the front frame is $T' = t'/(r_o/c)$ with $dT' = dT/\Gamma(T)$. The initial values at $T = T' = 0$ are $Z = 0$ and $U = V_1$. We also use the time $T'' = t''/(r_o/c)$ measured by a distant observer oriented at an angle $\theta_{obs} < \pi/2$ to the z -axis; $dT'' = dT[1 - U \cos(\theta_{obs})]$. Further, the observed time T''' for a cosmological source is given by $T''' = T''(1 + z)$ with z the redshift.

2.1. Number of Particles

The continuity equation for ions in the front frame is

$$\frac{\partial n'_i}{\partial t'} = -\frac{\partial(n'_i v')}{\partial z'} \quad (1)$$

where n'_i , v' , and t' are the number density, velocity, and time in the front frame. We integrate this equation over a

cylindrical 'pill box' of radius $r > r_j(z)$ and axial length $\Delta z'$ and use the Lorentz transformations to obtain an equation for the total number of ions in the front $N_i(T)$,

$$\frac{dN_i}{dT} = N_{io}[\Delta V_2 H(\Delta V_2) + \nu \Delta V_1 H(\Delta V_1)] \quad (2)$$

Here, $N_{io} \equiv \pi r^2 n_{i2}(z) r_o = \pi r_o^3 (n_{i2})_{z=0}$ is a constant by our earlier assumptions. Also, $H(x) = 1$ for $x > 0$ and $H(x) = 0$ for $x < 0$. If $\Delta z'$ were a constant, then we would have $\Delta V_1 = U - V_1$ and $\Delta V_2 = V_2 - U$, where upper case quantities are dimensionless. However, the plasma in the front expands freely with speed C'_s (normalized by c) so that $\Delta Z' = \Delta Z'_o + 2 \int_0^{T'} dT'' C'_s(T'')$, and this results in modified expressions for $\Delta V_{1,2}$. In the radial direction the plasma also expands freely with sound speed C'_s . C'_s is the compressional wave speed in the front frame. For the cases studied, C'_s is determined essentially by the particles in that the particle energy density is larger than that of the magnetic field. If both the ions and leptons are highly relativistic in the front frame, $C'_s = 1/\sqrt{3}$, whereas for non-relativistic ions but relativistic leptons $C'_s < 1/\sqrt{3}$. Magnetic pinching of the front is estimated to be small. Note that the number density of ions in the front frame is simply $n'_i = N_i/(\pi r_o^3 R^2 \Delta Z')$. The electric field in the front frame $|\mathbf{E}'|$ is small compared with $|\mathbf{B}'|$.

If $f_{li1} = f_{li2}$ and there is no $e\pm$ pair production in the front, then the total number of leptons in the front is simply $N_l = f_{li} N_i$. However, in the general case considered here,

$$\frac{dN_l}{dT} = N_{io}[f_{li2} \Delta V_2 H_2 + f_{li1} \nu \Delta V_1 H_1] + \frac{1}{\Gamma} \left(\frac{\delta N_l}{\delta T'} \right)_{e\pm} \quad (3)$$

where the H 's are the same as in equation (2). The main contribution to the pair production for the conditions considered is from collisions of synchrotron and SSC photons,

$$\left(\frac{\delta N_l}{\delta T'} \right)_{e\pm} = (\pi r_o^3 R^2 \Delta Z') r_o \times \int d\epsilon_1 \int d\epsilon_2 \frac{dn'_{syn}}{d\epsilon_1} \frac{dn'_{SSC}}{d\epsilon_2} \sigma_{pair} \Big|_{\epsilon_1 \epsilon_2 > (m_e c^2)^2}.$$

For rough estimates, we can write $\epsilon_1 = \frac{3}{2} \gamma^2 \hbar \omega'_o$, where $\omega'_o = e|B'|/(m_e c)$ is the cyclotron frequency in the front frame, and $\epsilon_2 = \gamma^2 \epsilon_1$. Thus, a rough condition for an electron to give pair production is $\gamma \geq \gamma_{pair} \equiv (mc^2/\hbar \omega'_o)^{1/3} \approx 3.5 \times 10^3 (10^3 G/|B'|)^{1/3}$. Electron-positron recombination is negligible for the conditions considered.

2.2. Momentum Conservation

In the front frame,

$$\frac{\partial T'_{0z}}{\partial t'} = -\frac{\partial T'_{zz}}{\partial z'} + \text{grav} + \text{rad} \quad (4)$$

where T'_{0z} and T'_{zz} are components of the energy momentum flux density tensor in the front frame, and 'grav' and 'rad' denote gravitational and radiative force contributions not included in T'_{ij} . We integrate (4) over the same pill box to obtain

$$(N_i m_i \bar{\gamma}_i + N_l m_e \bar{\gamma}_l) \Gamma^3 \frac{dU}{dT} = -\frac{\pi r_o^2 r_o}{c^2} [T'_{zz}] +$$

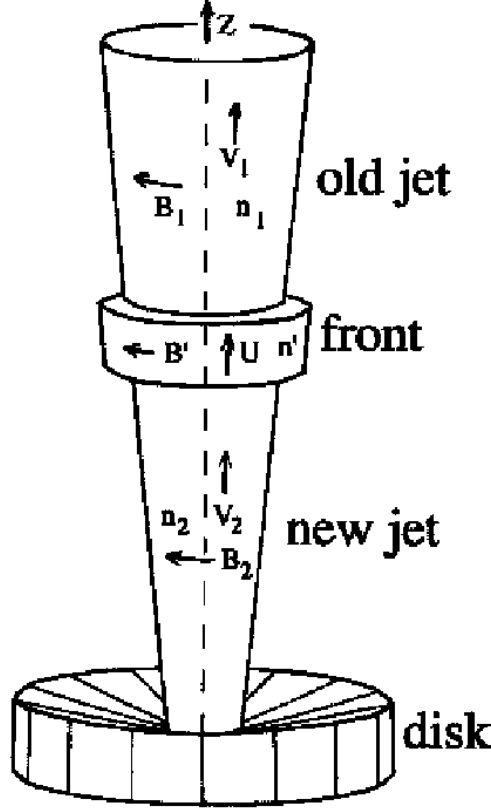


FIG. 1.— Sketch of the geometry of a propagating front in a Poynting flux jet.

$$\frac{r_o}{c^2} \int (grav + rad) . \quad (5)$$

$\bar{\gamma}_i$ and $\bar{\gamma}_l$ denote averages over the ion and lepton distribution functions in the *front frame*. In this frame the distributions are assumed isotropic and that for electrons is assumed the same as for positrons. The initial values of $\bar{\gamma}_i$ and $\bar{\gamma}_l$ are considered to be close to unity. A Lorentz transform gives $(T'_{zz})_s = \Gamma^2(T_{zz} - 2UT_{oz} + U^2T_{oo})_s$, where $s = 1, 2$. The lab frame components of the energy-momentum tensor for a Poynting flux jet are

$$\begin{aligned} T_{oo} = T_{zz} &= \frac{E_r^2 + B_\phi^2}{8\pi} = (1 + V^2)_s \left(\frac{B^2}{8\pi} \right)_s , \\ T_{oz} &= \frac{E_r B_\phi}{4\pi} = 2(V)_s \left(\frac{B^2}{8\pi} \right)_s , \end{aligned} \quad (6)$$

where $B = B_\phi$ at the edge of the jet. Thus, in equation (5) we have

$$\begin{aligned} -\frac{\pi r^2 r_o}{c^2} [T_{zz}] &= \frac{r^2 r_o B_2^2 \Gamma^2}{8c^2} \left\{ [(1 + U^2)(1 + V_2^2) - 4UV_2] - \right. \\ &\quad \left. b^2 [(1 + U^2)(1 + V_1^2) - 4UV_1] \right\} , \end{aligned} \quad (7)$$

where $b^2 \equiv (B_1/B_2)^2$, and $r^2 B_2^2 = \text{const} = r_o^2 (B_2)_{z=0}^2$. We assume $b^2 < 1$. The terms in the square brackets involving V_2 represent the push from the new Poynting jet, while those involving V_1 are for the push in the opposite direction from the old Poynting jet. A small modification of equation (7) similar to that of (2) is required to account for the free expansion of the plasma of the front. Note that the electromagnetic field contribution to the momentum of the front is small because $|\mathbf{E}'| \ll |\mathbf{B}'|$.

Dividing equation (5) by $\Delta M_o \equiv N_i(0)m_i + N_l(0)m_e$ gives

$$\begin{aligned} \left(\frac{N_i m_i \bar{\gamma}_i + N_l m_e \bar{\gamma}_l}{\Delta M_o} \right) \Gamma^3 \frac{dU}{dT} &= \mu \Gamma^2 \left\{ [(\dots)] \right\} + \\ \frac{r_o}{\Delta M_o c^2} \int (grav + rad) , \end{aligned} \quad (8)$$

where $\mu \equiv r_o^3 (B_2)_{z=0}^2 / (8\Delta M_o c^2) \gg 1$ is a dimensionless measure of the strength of the Poynting jet. The brackets $\{ \}$ denote the same quantity as in equation (7). The driving term $\propto \mu$ vanishes if both $\Gamma_1 \rightarrow \Gamma_2$ and $b \rightarrow 1$. If Γ, Γ_1 , and Γ_2 are all much larger than unity, it is clear from equations (7) and (8) that a steady state is possible if $b^2 > (\Gamma_1/\Gamma_2)^4$ (recall that $b^2 < 1$); that is, the push of

the old and new jets balance and the Lorentz factor of the front is $\Gamma = \Gamma_1[(1 - b^2)/(b^2 - (\Gamma_1/\Gamma_2)^4)]^{1/4}$. If b^2 is smaller than $(\Gamma_1/\Gamma_2)^4$, then no balance is possible and the Lorentz factor of the front Γ increases without limit.

The gravitational force in equation (8) can be written as $\int grav = -GM (N_i m_i + N_l m_e)/(r_o^2 + z^2)$. The radiative force depends in general on the geometry and energy distribution of the background radiation field of the central region of the AGN. Dermer et al. (1992) consider the case where the radiation comes from the disk, while Sikora et al. (1994) argue that the radiation field is from disk radiation scattered by a distribution of clouds orbiting the central object. We adopt a rough parameterization of the radiation fields of Dermer et al. and Sikora et al. The average photon energy is denoted $\bar{\epsilon}_{ph}$, the total luminosity L_{ph} , and the characteristic radius of the spatial distribution r_{ph} . The force due to this radiation field is $\int rad = (N_l \sigma_T) L_{ph} \mathcal{D}_{pz} \mathcal{F}_T / [\pi(r_{ph}^2 + (z - ar_{ph})^2)c]$, where $a = 0$ for the Dermer et al. model and $a = 1$ for that of Sikora et al. Here, $\mathcal{D}_{pz} = \Gamma^2[\cos(\theta_{ph}) - U]|\cos(\theta_{ph}) - U|$ is the Doppler factor which accounts for the change in the flux and the change in the z momentum of the photons between the lab and front frames, $\cos(\theta_{ph}) = (z - ar_{ph})/(r_{ph}^2 + (z - ar_{ph})^2)^{-1/2}$. σ_T denotes the Thomson cross section. The contribution of leptons with $\gamma > m_e c^2/\bar{\epsilon}_{ph}$ to $(N_l \sigma_T)$ in the radiative force is reduced in that the Klein-Nishina cross section applies. $\mathcal{F}_T = (1 - e^{-\tau_T})/\tau_T$ with $\tau_T = n'_l r_o R \sigma_T$ the Thomson optical depth of the front. For the conditions considered here, $\tau_T \ll 1$. For small axial distances, $\cos(\theta_{ph}) < U$, the radiative force acts as a drag whereas at larger distances it gives a push.

2.3. Energy Conservation

In the front frame,

$$\frac{\partial T'_{oo}}{\partial t'} = -\frac{\partial T'_{oz}}{\partial z'} - syn - ssc - Com, \quad (9)$$

where the last three terms represent the energy loss rates due to synchrotron radiation, inverse-Compton scattering off of synchrotron photons, and inverse-Compton scattering off of the above mentioned background photons. Following our previous method, we integrate (9) over the volume of the front to obtain

$$\Gamma \frac{d}{dT} \left[N_i (\bar{\gamma}'_i - 1) m_i + N_l (\bar{\gamma}'_l - 1) m_e + \frac{W'_B}{c^2} \right] = -\frac{\pi r_o^2 r_o}{c^3} [T'_{0z}] - \frac{r_o}{c^3} \int (syn + ssc + Com), \quad (10)$$

where $W'_B = (r_o^3/4c^2) R^2 \Delta Z' (B')^2$ is the magnetic field energy in the front. The magnetic field B' is discussed below in subsection 2.4. The driving term $\propto \mu$ vanishes if both $\Gamma_1 \rightarrow \Gamma_2$ and $b \rightarrow 1$. Because the acceleration process(es) in the front is not known, we make the well-known supposition (for example, Pacholczyk 1970) that the kinetic energy in the ions is a constant factor k times that in the leptons, $N_i (\bar{\gamma}'_i - 1) m_i = k N_l (\bar{\gamma}'_l - 1) m_e$. As a result, $\bar{\gamma}'_i$ is determined in terms of $\bar{\gamma}'_l$. Therefore, in the following γ without a subscript refers always to the lepton Lorentz factor.

A Lorentz transform gives $T'_{oz} = \Gamma^2[(1 + U^2)T_{oz} - UT_{oo} - UT_{zz}]$, so that

$$-\frac{\pi r_o^2 r_o}{c^3} [T'_{0z}] = \frac{r_o^2 B_2^2 \Gamma^2}{4c^2} \left\{ [(1 + U^2)V_2 - U(1 + V_2^2)] H_2 - b^2 [(1 + U^2)V_1 - U(1 + V_1^2)] H_1 \right\}. \quad (11)$$

Dividing equation (10) by ΔM_o gives

$$\frac{\Gamma}{\Delta M_o} \frac{d}{dT} \left[N_l (\bar{\gamma}_l - 1) (1 + k) m_e + \frac{W'_B}{c^2} \right] = 2\mu \Gamma^2 \left\{ [(\dots)] - \frac{r_o}{\Delta M_o c^3} \int (syn + ..) \right\}, \quad (12)$$

where the brackets $\{\}$ denote the same quantity as in equation (11). The driving term $\propto \mu$ vanishes if both $\Gamma_1 \rightarrow \Gamma_2$ and $b \rightarrow 1$.

The synchrotron energy loss rate in the front frame is:

$$\int syn = \frac{32\pi}{9} r_e^2 N_l \overline{(\gamma)^2} c \left(\frac{B'}{8\pi} \right)^2 \mathcal{F}_{syn}, \quad (13a)$$

where $r_e \equiv e^2/(m_e c^2)$ is the classical electron radius, and $\overline{(\gamma)^2} = \int_{\gamma_1}^{\infty} d\gamma \gamma^2 f_l / N_l$, where γ_1 is the Lorentz factor below which synchrotron self-absorption becomes strong as discussed below. $\mathcal{F}_{syn} = [1 - \exp(-\tau_{syn})]/\tau_{syn}$ is synchrotron opacity factor with τ_{syn} the optical depth for synchrotron photons (Pacholczyk 1970). The synchrotron-self-Compton energy loss rate is:

$$\int ssc = \frac{4}{3} (N_l \sigma_T) \overline{(\gamma)^2} c \left(\frac{64 N_l \overline{(\gamma)^2} \sigma_T}{9 r_o^2 R \Delta Z'} \right) \left(\frac{B'}{8\pi} \right)^2 \mathcal{F}_{syn}. \quad (13b)$$

The energy loss rate in the front frame due to Compton scattering off of the background photons is:

$$\int com = \frac{4}{3} (N_l \sigma_T) \overline{(\gamma)^2} c (\mathcal{U}'_{ph}) \mathcal{F}_T, \quad (13c)$$

where $\mathcal{U}'_{ph} = L_{UV} \mathcal{D}_{ph}^2 / [\pi r_o^2 c (R_{ph}^2 + (Z - a R_{ph})^2)]$ is the background photon energy density in the front frame, and $\mathcal{D}_{ph} = \Gamma[1 - U \cos(\theta_{ph})]$ is the Doppler factor for photons in the front frame relative to the disk.

2.4. Magnetic Flux Conservation

The magnetic field in front frame B' is determined by taking into account the influx of magnetic flux with the new jet matter (subscript 2) and the old jet matter (subscript 1). We let $\Phi' = R \Delta Z' B'$ denote the toroidal flux (in Gauss) in the front. Then

$$\frac{d\Phi'}{dT} = B_o [\Delta V_2 H(\Delta V_2) + b \Delta V_1 H(\Delta V_1)], \quad (14)$$

where $B_o \equiv (B_2)_{z=0}$ and the H 's are the same as in equation (2). If $b < 0$, there is annihilation of magnetic flux in the front (see Romanova and Lovelace 1992; and Lovelace, Newman, and Romanova 1996).

2.5. Lepton Distribution

The lepton distribution function suggested by observations has a hard power law form in the main energy containing range, say, $f_l = K_1/\gamma^2$ for $\gamma_1 \leq \gamma \leq \gamma_2$ with $1 \ll \gamma_1 \ll \gamma_2$. For $\gamma \geq \gamma_2$, the distribution is steeper,

say, $f_l = K_2/\gamma^3$, and at even larger energies, $\gamma \geq \gamma_3$, f_l is even steeper. For $\gamma < \gamma_1$, f_l is assumed negligible (see Figure 2). Thus, f_l is characterized mainly by γ_1 and γ_2 . We have $\bar{\gamma} = \gamma_1[1 + \ln(\gamma_2/\gamma_1)]$, and $\bar{\gamma}^2 = \mathcal{C}\gamma_1\gamma_2$, with $\mathcal{C} = 1 + \ln(\gamma_3/\gamma_2)$. The relevant value of γ_1 is the Lorentz factor below which synchrotron self-absorption becomes strong. Self-absorption as treated for example by Pacholczyk (1970) then gives $\gamma_1 = \gamma_1(B', n'_l, R)$. With γ_1 known, we have $\gamma_2 = \gamma_1 \exp(\bar{\gamma}/\gamma_1 - 1)$. The value of \mathcal{C} depends only weakly on γ_3/γ_2 and we take $\gamma_3/\gamma_2 = \bar{\gamma}/\gamma_1$.

3. RESULTS

Equations (2), (3), (8), (12) and (14) have been solved numerically to obtain the time dependences of the physical variables. Here, we first discuss the time-dependences for a reference case where the black hole mass $M = 10^9 M_\odot$ so that $r_o = 8.9 \times 10^{14}$ cm, $\mu = r_o^3(B_2)_{z=0}^2/(8\Delta M_o c^2) = 15$, $B_o = 10^3$ G, $b = |B_1/B_2| = 0.5$, $\Gamma_1 = 8$, $\Gamma_2 = 18$, $\nu = n_{i1}/n_{i2} = 0.44$, $k = 1$, and the initial lepton-ion ratio $f_{li}^o = 5$. For the background photons, $L_{UV} = 10^{46}$ erg/s, $\bar{\epsilon}_{ph} = 10$ eV, $r_{ph} = 0.1$ pc, and $a = 0$. The angle between the observer and the jet axis is $\theta_{obs} = 0.1$ rad. All results are presented for the dependence on time (t'') seen by a distant observer where it is recalled that $dt'' = dt[1 - U\cos(\theta_{obs})]$. The redshift dependences are not included in the equations.

3.1. Time Dependences

The velocity of the front U , initially equal to V_1 , increases rapidly and approaches the equilibrium value U_∞ which corresponds to the bulk Lorentz factor $\Gamma_\infty = 10$. This is shown in Figure 3. The apparent velocity of the front (with respect to the nucleus) $V_{app} = U \sin(\theta_{obs})/[1 - U\cos(\theta_{obs})]$ approaches 9.9. The Doppler boost factor $\delta = 1/[\Gamma(1 - U\cos(\theta_{obs}))]$ approaches 10.

The total number of ions in the front grows with time, because under most conditions the front moves faster than the old jet matter and slower than the new jet matter, thus accumulating particles from both sides. This is shown in Figure 4. For the case shown there is no pair production. Thus, the ratio of leptons to ions f_{li}^o decreases with time and approaches unity. Other cases were calculated where pairs are created and the number of leptons grows so that f_{li} becomes much larger than its initial value.

Although the total number of particles in the front grows with time, the number densities decrease with time due to the expansion of the volume of the front. This is shown in Figure 5. The number densities of synchrotron, SSC, background, and inverse-Compton photons in the front also decrease with time as shown in Figure 5.

Figure 6 shows the evolution of the different characteristic Lorentz factors, γ_1 , γ_2 , and γ_3 , of the lepton distribution. Initially, the leptons are assumed to have the same small energy corresponding to a Lorentz factor $\gamma = 1.01$. Later, when the average lepton Lorentz factor ($\bar{\gamma}$) becomes larger than that corresponding to self-absorption (γ_1), a complete spectrum forms extending from γ_1 to γ_3 . Initially, γ_1 , γ_2 , and γ_3 grow rapidly and later more slowly. The top curve in Figure 6, γ_{pair} , corresponds to the energy of leptons at which pair creation sets in.

The total apparent luminosities due to synchrotron, SSC, and Compton processes for a distant observer at an

angle θ_{obs} to the line of sight are calculated including the solid angle boost factor δ^2 between the front frame and the observer, where $\delta = [\Gamma(1 - U\cos(\theta_{obs}))]^{-1}$. These are shown in Figure 7. At early times in an outburst, the SSC radiation predominates because the magnetic field in the front is strong and the number of synchrotron photons is higher than that of background photons. Later, the magnetic field in the front decreases and thus the background photons predominate. At the same time, the leptons are accelerated in the front and consequently inverse-Compton radiation grows, and then later decreases. The time of the peak of the inverse-Compton emission depends approximately linearly on the radius r_{ph} of the background photon distribution. Synchrotron radiation is at much lower luminosity during the first part of the front propagation. The dependences of the maximum luminosities of the different processes are discussed later.

The observed frequency is boosted by a factor δ . The frequencies of radiation corresponding to different processes and to the characteristic values γ_1 , γ_2 , and γ_3 of the lepton distribution, are shown in Figure 8. One can see that the radiation of the front covers most of the frequency range from the self-absorption limit (the lowest curve), up to high gamma ray energies. In many bands of the spectrum, there are contributions from two processes. For example, in the Egret band (from $10^{22.5}$ Hz to $10^{24.5}$ Hz) we typically have contributions from both inverse-Compton and SSC radiation. Initially, synchrotron radiation contributes to the band from IR to UV, SSC covers the range of frequencies from soft X-ray to EGRET GeV energies, and the inverse-Compton covers the range from the high-energy X-ray to the EGRET GeV energies. Thus, during an EGRET high-energy flare one may expect almost simultaneous flashes in wavebands from IR to very high energies, excluding the radio band which is initially self-absorbed.

3.2. Dependences of Maxima of Flares

The maxima of the total apparent luminosities due to inverse-Compton (L_{Com}), synchrotron-self-Compton (L_{SSC}) and synchrotron processes (L_{syn}) depend on the parameters θ_{obs} , B_o , μ , M , f_{li}^o , r_{ph} , and L_{UV} approximately as

$$\begin{aligned} L_{Com} &\sim 1.7 \times 10^{47} \left(\frac{0.1}{\theta_{obs}}\right)^{1.8} \left(\frac{\mu}{20}\right)^{1.4} \left(\frac{M}{10^9 M_\odot}\right)^{1.0} \times \\ &\left(\frac{B_o}{10^3 G}\right)^{1.8} \left(\frac{10}{f_{li}^o}\right)^{1.4} \left(\frac{0.1 pc}{r_{ph}}\right)^{1.0} \left(\frac{L_{UV}}{10^{46} ergs/s}\right)^{1.0} \frac{ergs}{s}, \\ L_{SSC} &\sim 2.4 \times 10^{47} \left(\frac{0.1}{\theta_{obs}}\right)^{1.8} \left(\frac{\mu}{20}\right)^{2.4} \left(\frac{M}{10^9 M_\odot}\right)^{3.1} \times \\ &\left(\frac{B_o}{10^3 G}\right)^{5.7} \left(\frac{10}{f_{li}^o}\right)^{2.5} \frac{ergs}{s}, \\ L_{syn} &\sim 1.6 \times 10^{46} \left(\frac{0.1}{\theta_{obs}}\right)^{1.8} \left(\frac{\mu}{20}\right)^{1.3} \left(\frac{M}{10^9 M_\odot}\right)^{2.2} \times \\ &\left(\frac{B_o}{10^3 G}\right)^{3.8} \left(\frac{10}{f_{li}^o}\right)^{1.3} \frac{ergs}{s}, \end{aligned} \quad (15)$$

if the parameters are of the order of the normalization values.

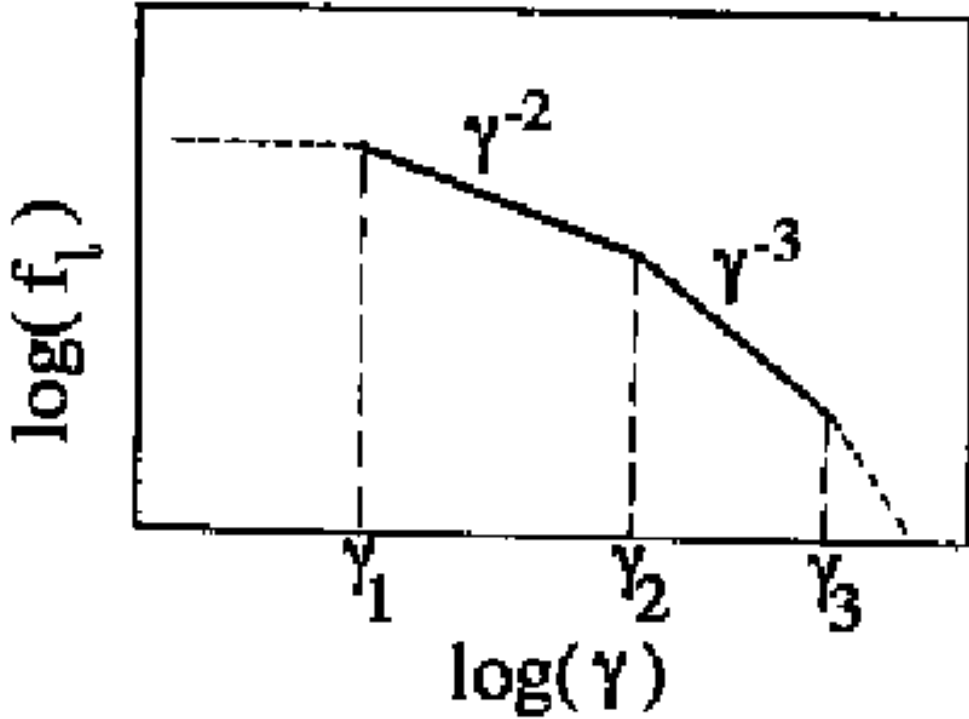


FIG. 2.— Lepton distribution function in the comoving frame of the front. γ_1 , γ_2 , and γ_3 are derived from the equations of Section 2.

The dependences on μ in equation (15) are approximately valid for $10 \leq \mu \leq 50$. For $\mu < 10$, the power is higher for SSC and synchrotron radiation, but the same for Compton radiation. For $\mu > 50$, the luminosities go to a constant. The dependences on B_o are valid for $B_o < 2000$ G, and become flatter for stronger fields. The dependence on f_{li}^o is about the same as in equation (15) for $5 < f_{li}^o < 15$, and becomes steeper for SSC and synchrotron radiation for $f_{li}^o > 15$ and does not depend on f_{li}^o for $f_{li}^o < 4$. As for the dependences on θ_{obs} , the L 's depend more strongly on θ_{obs} than in equation (15) at larger angles ($\theta_{obs} > 0.1$) and more weakly for smaller angles. The dependence on M is approximately the same at all parameter ranges.

Notice that the shape of the light curves are quite different for different parameters. There are several possibilities: **(1)** Both SSC and Compton radiation may be in the EGRET band. Then, the shape of the EGRET light curve is determined essentially by the SSC radiation which gives a fast rise of luminosity with typical time scale of growth $t'' = 0.03$ days = 43 min (see Figure 9a). The rise time may of course be slower due to a more gradual transition from the old jet to the new. **(2)** SSC radiation frequencies may be lower than the EGRET band so that only Compton radiation is observed. Then, the light curve shape will be determined by Compton radiation with a maximum at $t'' = 0.13$ days for our reference values (see Figure 9b). **(3)** No radiation may fall in the EGRET band. For example, changing μ (with other

parameters fixed) we get a sharp SSC flare for $\mu > 35$, a flatter Compton flare for $20 < \mu < 35$, and no radiation in the EGRET band for $\mu < 20$. Thus, for this set of parameters, the value μ , which is the initial ratio of magnetic to rest mass energy-density, should be relatively high. The shape of the EGRET light curves also depends, for example, on the initial ratio of leptons to ions. For $1 < f_{li}^o < 5$, SSC type flares predominate. For $5 < f_{li}^o < 15$, Compton type flares predominate, and for $f_{li}^o > 15$, no radiation falls in the EGRET band. Thus, the shape of the flare may be different in different sources or may change in the same source between different outbursts, depending on the magnetic/particle rest mass energy-density ratio, or on the initial ratio of leptons to ions in the front plasma.

The maxima of the flares in the SSC and synchrotron radiation occur very soon after outburst (much less than a day). The maximum of the inverse-Compton flare is much later and may be observable,

$$t''_{Com} = 0.13 \left(\frac{\theta_{obs}}{0.1} \right)^{0.9} \left(\frac{10}{\mu} \right)^{0.1} \left(\frac{f_{li}^o}{10} \right)^{0.1} \left(\frac{r_{ph}}{0.1 pc} \right), \quad (16)$$

in days. Note that t''_{Com} has essentially no dependence on M .

Later, after the maxima, all luminosities decrease. The SSC luminosity decreases as $L_{SSC} \sim (t'')^{-2}$, the synchrotron luminosity as $L_{syn} \sim (t'')^{-1}$, and the inverse-Compton luminosity as $L_{Com} \sim (t'')^{-4}$ for $t'' < 2 - 3$

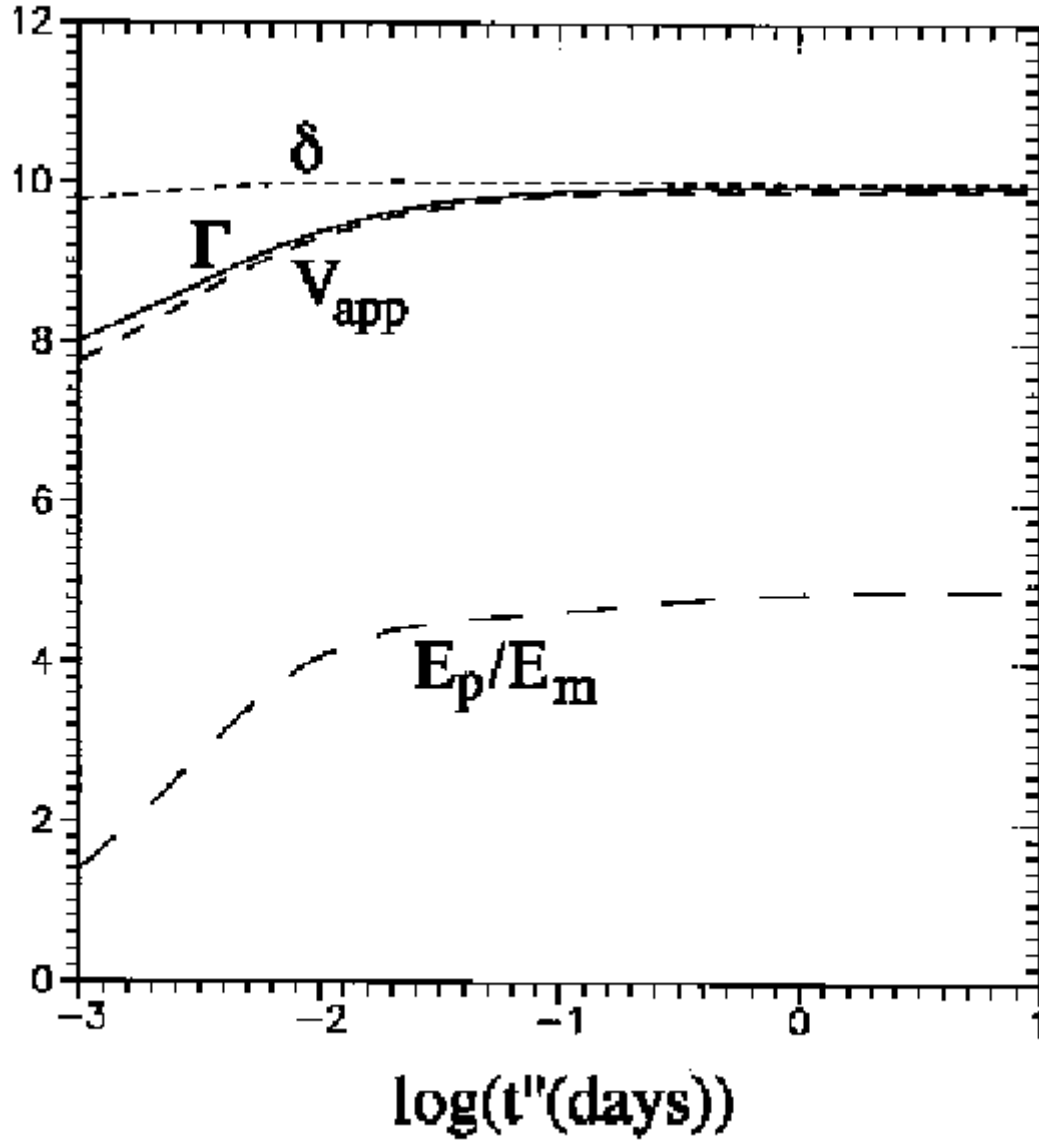


FIG. 3.— Bulk Lorentz factor Γ , apparent velocity of the front v_{app} (normalized to c), and Doppler boost factor δ versus time measured by a distant observer for the reference parameters given in Section 3.

days, but later for $t > 15$ days it flattens to $\sim (t'')^{-1}$.

The rise of the inverse-Compton luminosity is determined by the growth of the number and energy of leptons in the front. The front is transparent to inverse-Compton radiation from the beginning. At the same time, initially plasma of the front is opaque to the synchrotron photons, and the rapid growth of synchrotron and SSC radiation is determined by the fact that plasma becomes transparent to synchrotron photons. The decline of inverse-Compton radiation is due to the fact that the energy density of background photons decreases in the front frame. An important factor in the decrease is the Doppler shift of the background photons relative to the front for $Z > R_{ph}$. As for synchrotron and SSC radiation, they decrease with time because the magnetic field in the front decreases with time.

4. COMPARISON WITH OBSERVATIONS

4.1. *Gamma-Ray Variability: Comparison with the Flare in PKS 1622-297*

Here, we compare theoretical and observed light curves. The luminosity in the EGRET band ($10^{22.5} - 10^{24.5}$) Hz is determined in general by both inverse-Compton and SSC processes. We integrated the gamma radiation in the EGRET band and got two qualitatively different types of light curves (Figures 9a and 9b). The difference is determined by the fact that in some cases (depending on parameters) SSC radiation is below the EGRET frequency limit and the light curve is determined by the inverse-Compton light curve (see Figure 9b). In the opposite case, when the SSC radiation is within the EGRET band, the light curve is determined by both processes, but the SSC radiation has a strong peak at small time scales, and this determines the shape of the light curve (Figure 9a). In the first case, it is more probable to observe the fast rise and gradual decrease of gamma luminosity, compared with the second case, where the rise of luminosity is so fast (maximum reached at $t'' = 0.02$ days) that it will be difficult to observe and only the ‘tail’ of the flare will be seen (see, however, Mattox et al. 1996).

EGRET observations of gamma-ray blazars show different types of flares. In some cases the growth of the luminosity is relatively slow compared with the decay (Kniffen et al. 1993). In other cases (for example, Hartman et al. 1993), only a decaying light curve is observed during the EGRET set of observations. In the third type of flare, the rise of the luminosity is much faster than the decay (Mattox et al. 1996).

Time resolved observations of the brightest observed gamma-ray flare from blazar PKS 1622-29 (Mattox et al. 1996) show that during the main flare the flux increases by an order of magnitude on a 2 hour time scale, whereas the decay is on a 7 hour time scale. Thus the rise is faster than the decay. We fitted this flare by a ‘Compton type’ flare using the parameters: $M = 3 \times 10^9 M_\odot$, $B_o = 1700$ G, $\theta_{obs} = 0.1$ rad $= 11.5^\circ$, $\mu = 20$, $f_{li}^o = 6$, $r_{ph} = 0.3$ pc, $\bar{\epsilon}_{ph} = 10$ eV, $L_{UV} = 2 \times 10^{46}$ ergs/s, and $a = 1$. This is shown in Figure 10. For calculation of the theoretical flux we used standard formulae for the luminosity distance at the redshift of the source $z = 0.815$, Hubble’s constant $H_o = 75$ km/s/Mpc, and a cosmological parameter $q_o = 1/2$. Also, we took into account the cosmological redshift

of the frequencies and the dilation of the time scale of the outburst. The value $a = 1$ of Figure 10 corresponds to background photons scattered by clouds (Sikora et al. 1994), and it gives a more symmetric Compton flare than $a = 0$. We also obtained fits to the PKS flare with $a = 0$ where the background photons come from the disk (Dermer et al. 1992).

The fit of our model to the PKS 1622-29 data is not unique, but the fitting in all cases requires a relatively massive black hole ($M > 10^9 M_\odot$) and a relatively strong magnetic field at the base of the jet ($B_o > 10^3$ G). Also, it appears necessary to have an initial ratio of magnetic field to rest mass energy-density large compared with unity, $\mu \sim 10 - 30$. Note that the quasar PKS 1622-297 is the brightest gamma-ray quasar (Mattox, et al., 1996). In other lower gamma luminosity blazars, M and/or B_o may be smaller.

The appearance of one type of flare or another, and also the strength of the flares, depends on values of the plasma parameters (f_{li}^o , μ , B_o) which may be random. Flares where the stage of growth is very short may be explained by ‘spike’ type SSC flares (Figure 9a), whereas the slower rising gamma light curves may be inverse-Compton flares (Figure 9b). Note, that the fast growth and decay of luminosity in the beginning of the strong PKS 1622-29 flare may be connected with ‘spike’ type SSC flare, which appears at smaller initial lepton-ion number ratios ($f_{li}^o < 5$).

In the present model, we proposed that the new Poynting jet pushes matter continuously. However, if the push decreases with time, then the front will lose energy as a result of radiation and the luminosity will decrease more rapidly than that show here. This effect may also explain rapid decay, compared with growth, of the prominent flare of the quasar 3C 279 (Kniffen et al. 1993).

4.2. *Radio Variability*

Analysis of the correlation between gamma-ray flares and those in radio emissions at short time scales has shown that there is no direct correlation in most blazars (Reich et al. 1993). Moreover, often the radio flux is in the low state during the gamma-ray flare. However, observations on longer time-scales show that after strong flares in the EGRET band, the radio luminosity starts to grow and has a maximum several months later than the gamma-ray flare (Reich et al. 1993). This may result from either synchrotron self-absorption or free-free absorption by plasma surrounding the source core (Matveyenko et al. 1992). Thus, the radio emission appears at later times when the density in the front and/or the external density are much lower.

In our model the synchrotron self-absorption frequency is initially in the infrared or UV, depending on parameters. Thus, initially, there is no radio emission from the front. Later, the self-absorption frequency $\nu_1(syn)$ slowly decreases (Figure 8) and goes to ~ 3 mm (10^{11} Hz) after several days. Much later, $\nu_1(syn)$ falls into the cm radio band. For some parameters of the model, the millimeter emission appears one or two weeks after the flare. Initially, only a small fraction of the total luminosity goes into low frequencies, and the radio flux is very small. Because of the slow decrease of $\nu_1(syn)$ with time, $\nu_1(syn) \sim 10^{12}(t'')^{-1}$ Hz, the maximum of the radio luminosity may be a few months later than the gamma-ray

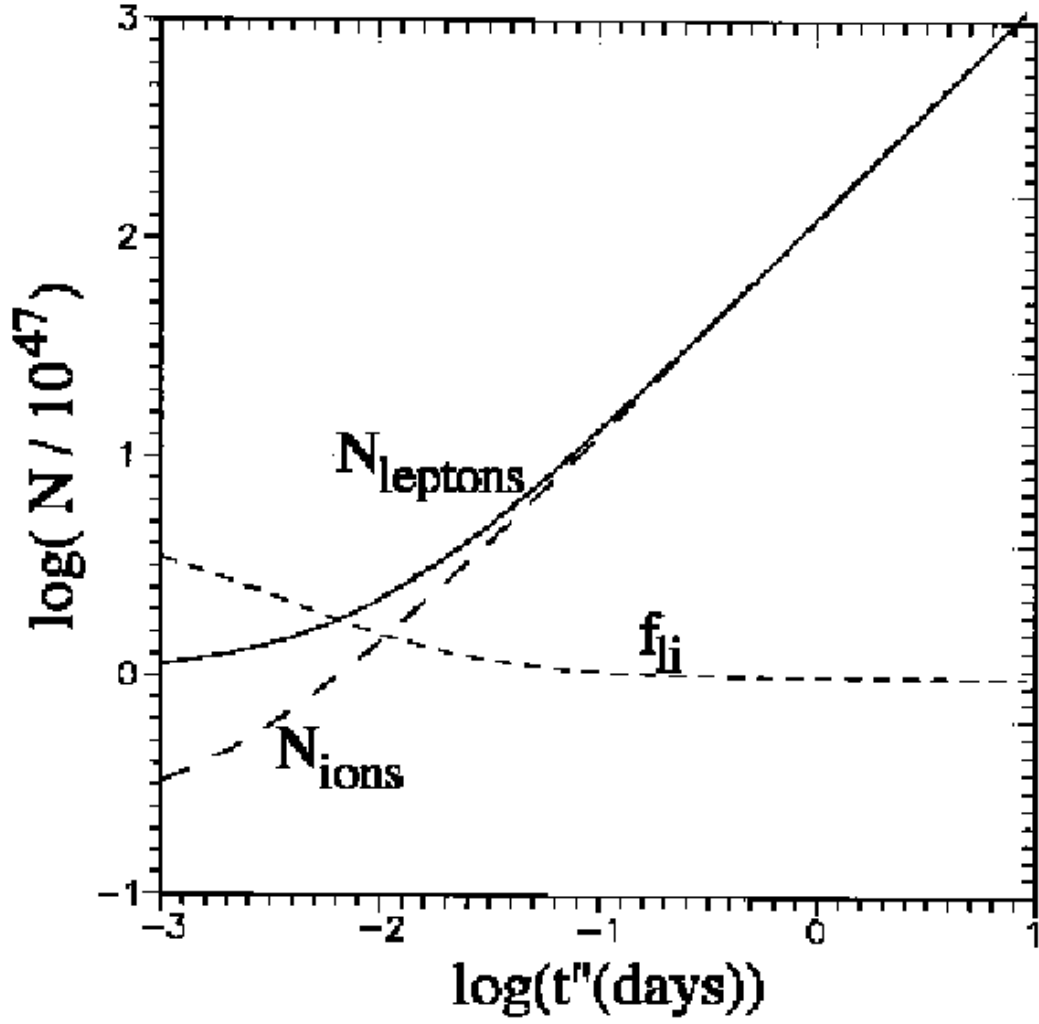


FIG. 4.— Total number of leptons N_l and ions N_i in the front and their ratio f_{li} versus time measured by distant observer.

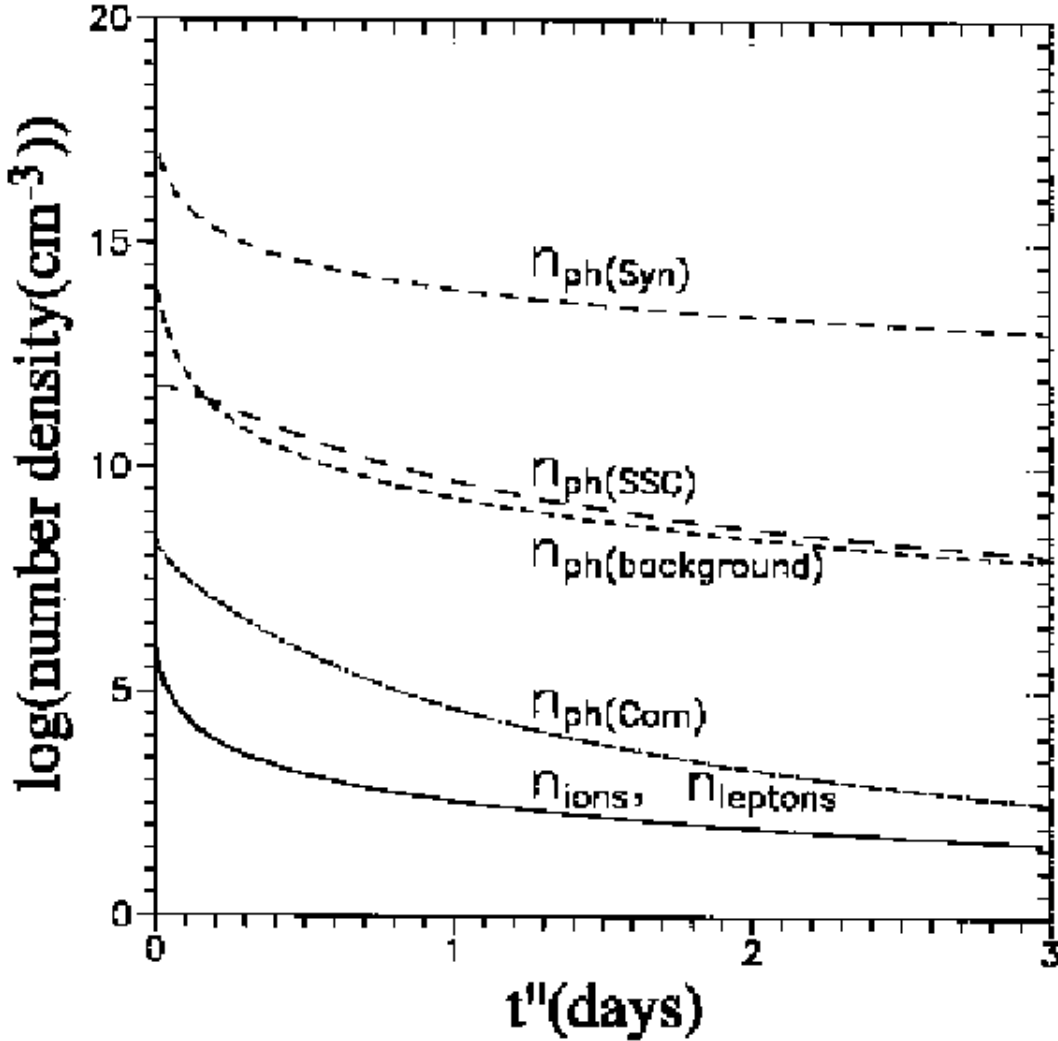


FIG. 5.— Number density of leptons n'_l , ions n'_i , background photons n'_{ph} , synchrotron photons n'_{syn} , synchrotron-self-Compton photons n'_{SSC} and inverse-Compton photons n'_{Com} (in units of cm^{-3}) in the front frame versus the logarithm of time measured by distant observer.

flare. Here, we did not take into account possible free-free absorption of radio waves by distributed plasma in the core of the source exterior to the jet. This absorption may also contribute to the delay in the appearance of the radio emission.

The present model of a propagating front in a Poynting flux jet is similar in some respects to the model of radio variability of Aller, Aller, and Hughes (1985) and Hughes, Aller, and Aller (1985) based on weak shocks propagating along a hydrodynamic jet. Detailed multi-frequency radio observations of the quasar 0528+134 shows that after a strong gamma-ray flare, the radio flux grows and has a maximum few months later (Pohl et al. 1995). It is important to note that during this event, the new VLBI super-luminal component appeared with a back-extrapolated time of origin close to the time of the gamma-ray flare (Krichbaum et al, 1995). These observations support the present model where a strong impulsive disturbance - the front - propagates along and is powered by an otherwise invisible Poynting flux jet. The

front radiates first in gamma rays, and later becomes strong in the radio when it is observed as a new super-luminal VLBI jet component.

5. CONCLUSIONS

The paper develops a self-consistent dynamical model of gamma-ray flares and VLBI outbursts of blazars based on lepton acceleration in the propagating front of an otherwise invisible Poynting flux jet. Inverse-Compton scattering of the accelerated, relativistic leptons off of background photons as well as off of synchrotron photons (the SSC process) and synchrotron radiation are taken into account.

It is shown that gamma-ray flares in the frequency band of the EGRET instrument (at $50 < E < 10^4$ MeV) may be of two types: (1.) ‘SSC spikes’ which have a fast rise (\sim hr.) and gradual decay of luminosity. This type of flare appears in the cases where SSC photons have high enough energy to be in the EGRET band. In this case inverse-Compton radiation, which usually gives a smaller

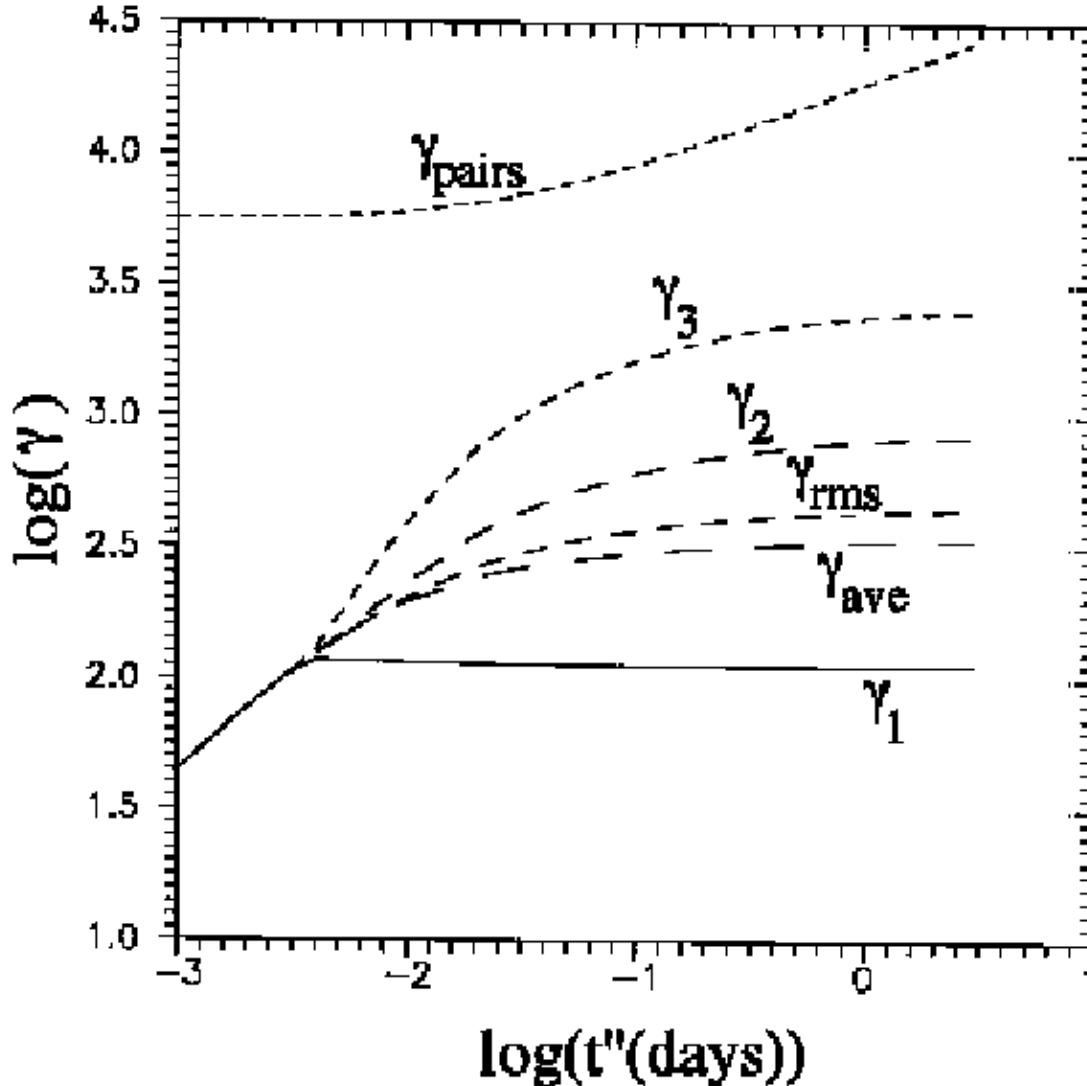


FIG. 6.— Lorentz factors in the front frame separating different parts of the lepton spectrum: γ_1 , γ_2 , and γ_3 versus time measured by distant observer. $\bar{\gamma}$ is the average Lorentz factor. γ_{rms} is the the root mean square Lorentz factor. γ_{pairs} is the threshold Lorentz factor for pair production. For the case shown there is no pair production.

contribution to the luminosity, is hidden by the strong SSC flare. (2.) ‘Compton flares’ which have a growth time of few hours and a duration of days up to weeks (depending on the distribution of background photons and viewing angle). Comparison with recent observations of the gamma-ray flare in PKS 1622-297 (Mattox et al. 1996) show that it may be interpreted as a ‘Compton flare’. To explain the high luminosity and the short duration of the PKS flare, the viewing angle must be quite small, $\theta_{obs} \sim 0.1$ rad. Also, we need a black hole mass $M \sim 3 \times 10^9 M_\odot$ and a magnetic field at the base of the jet $B_o \sim 10^3$ G.

The model gives almost simultaneous flares for photon energies from high-energy gamma-ray to lower energy gamma, X-ray, UV, visible, and down to the infrared. The short wavelength (mm) radio flare for some parameters may appear shortly (\sim days) after the main gamma flare, because the self-absorption frequency, which ini-

tially corresponds to the IR region of spectrum, decreases rapidly during a few days (see Figure 8) to short wavelength radio band (in some cases, however, mm radiation may appear much later). Later, it decreases more slowly, so that the centimeter waveband radio radiation in most of the cases should appear much later (\sim months) than the gamma-ray flare.

In many gamma ray loud objects, both flares and steady radiation are observed (Fichtel and Thompson 1994; Montigny et al. 1995). The steady radiation may come from a superposition of a number of overlapping outbursts. In other cases, the EGRET instrument detects only the highest states of strong flares with the weaker steady emission obscured in the noise.

Extremely high energy photons (\sim TeV) have been detected from the object Markarian 421 (Punch et al. 1992). Here, we comment on the possible origin of TeV photons in the framework of the present model. TeV

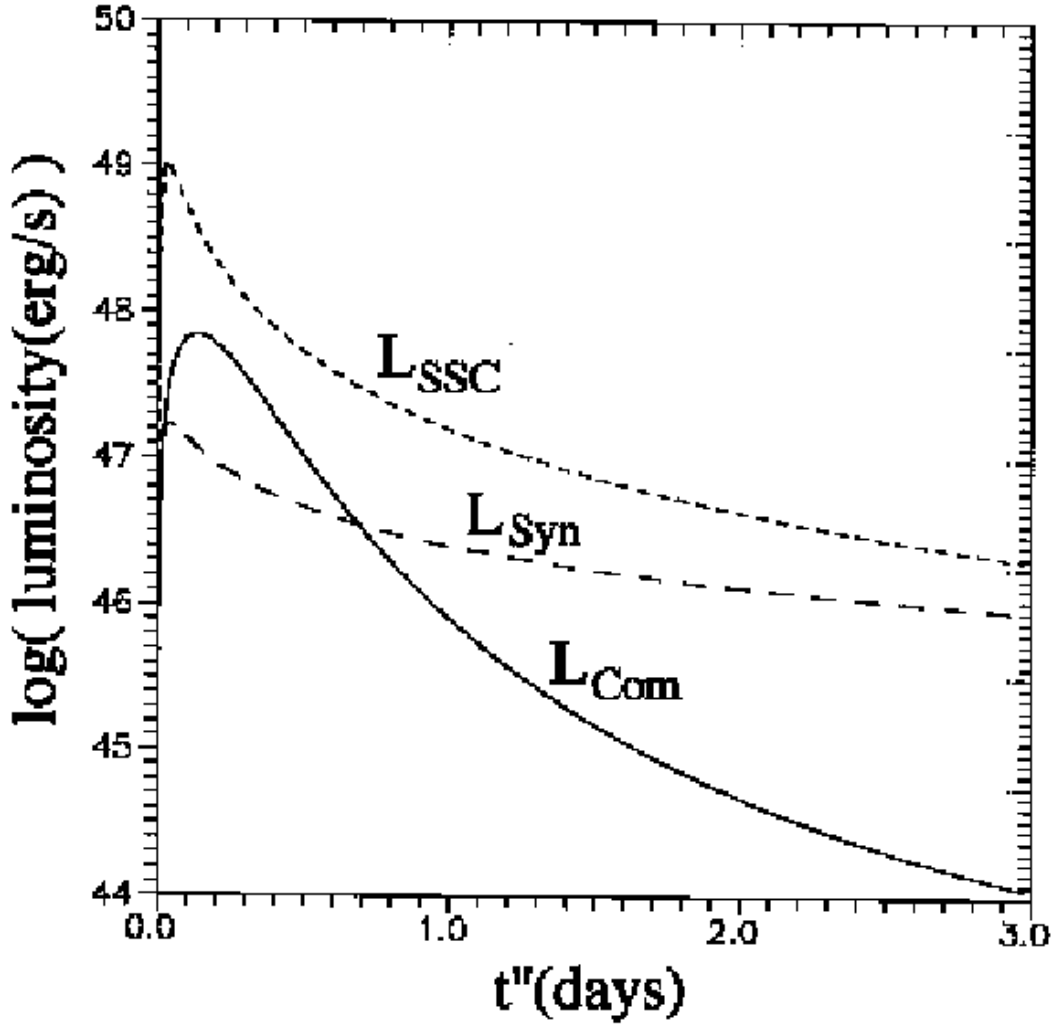


FIG. 7.— Total (bolometric) apparent luminosities radiated by the front due to the inverse-Compton, SSC, and synchrotron processes (in *erg/s*) as a function of time measured by distant observer.

radiation may result from the SSC process by lepton scattering off of synchrotron photons if the lepton distribution function extends to sufficiently high Lorentz factors ($\sim 10^5$). However, the magnetic field at the base of the jet B_0 may have to be smaller than the values considered here ($\sim 10^3$ G) in order to avoid excessive pair production.

Both authors were supported in part by NSF grant

AST-9320068. MMR was also supported in part by Russian Fundamental Research Foundation Grant No 93-02-17106 and by the Scientific and Educational Center of Kosmomicrophysics "KOSMION". We thank Drs. J.R. Mattox, T.P. Krichbaum, and A. Levinson for stimulating discussions.

REFERENCES

- Aller, H.D., Aller, M.F., and Hughes, P.A. 1985, *ApJ*, 298, 296
 Blandford, R.D. 1993, in *Compton Gamma-Ray Observatory*, AIP Proceedings No. 280, eds. M. Friedlander, N. Gehrels, & D.J. Macomb (New York: AIP), p. 533
 Burns, M.L., & Lovelace, R.V.E. 1982, *ApJ*, 262, 87
 Coppi, P.S., Kartje, J.F., & Königl, A. 1993, in *Compton Gamma-Ray Observatory*, AIP Proceedings No. 280, eds. M. Friedlander, N. Gehrels, & D.J. Macomb (New York: AIP), p. 559
 Dermer, C.D., Schlickeiser, R., & Mastichiadis, A., 1992, *A&A*, 256, L27
 Fichtel, C.E. & Thompson, D.J. 1994, in *High Energy Astrophysics*, J.M. Matthews, ed. (World Scientific: Singapore), p. 1
 Ghisellini, G., & Madau, P. 1996, *ApJ*, in press
 Hartman, R.C., Bertsch, D.L., Fichtel, C.E., Hunter, S.D., Kanbach, G., Kniffen, D.A., Kwok, P.W., Lin, Y.C., Mattox, J.R., Mayer-Hasselwander, H.A., Michelson, P.F., von Motigny, C., Nel, H.I., Nolan, P.L., Pinkau, K., Rothermel, H., Schneid, E., Sommer, M., Sreekumar, P., Thompson, D.J. 1992, *ApJ*, 385, L1

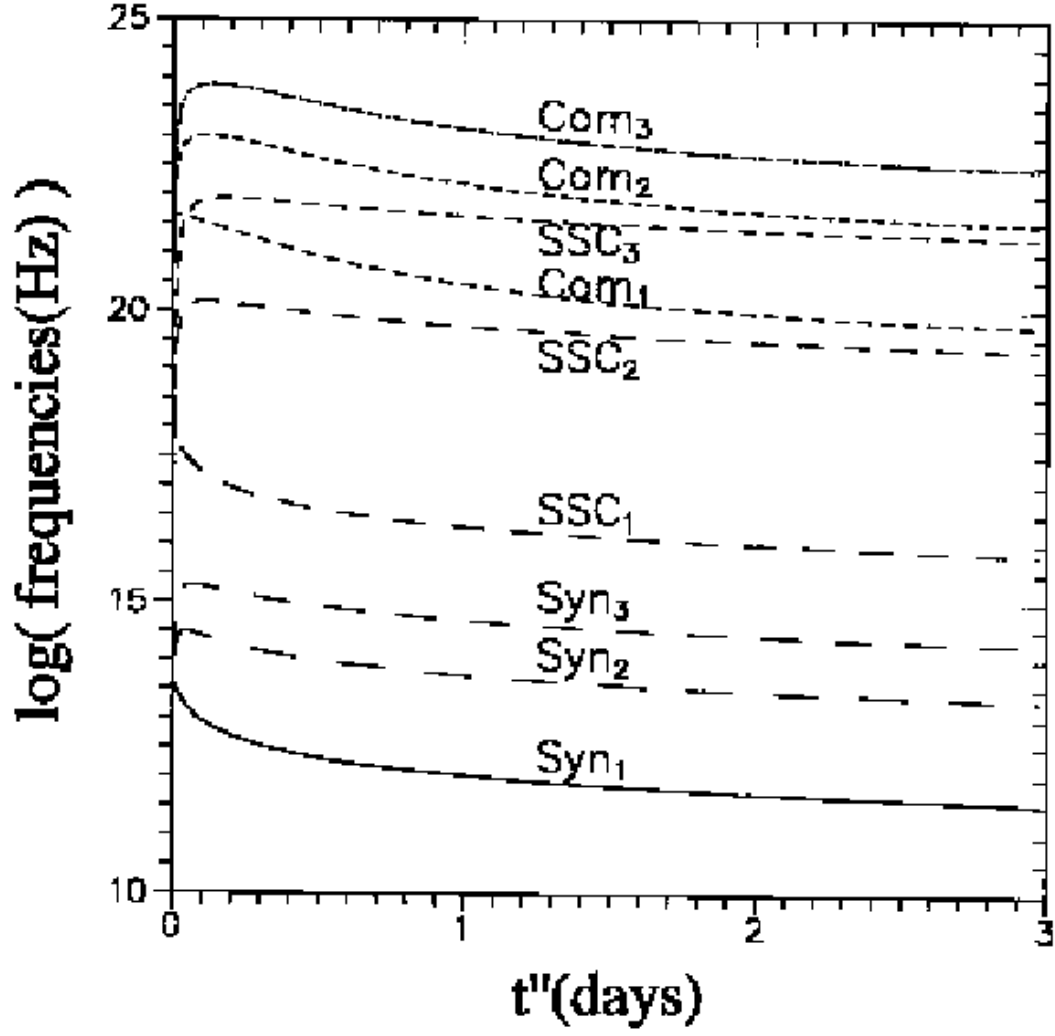


FIG. 8.— Apparent frequencies in Hz of radiation generated by electrons with Lorentz factors γ_1, γ_2 , and γ_3 due to the synchrotron, SSC, and inverse-Compton processes as a function of time measured by distant observer.

- Hartman, R.C., Bertsch, D.L., Dingus, B.L., Fichtel, C.E., Hunter, S.D., Kanbach, G., Kniffen, D.A., Lin, Y.C., Mattox, J.R., Mayer-Hasselwander, H.A., Michelson, P.F., von Montigny, C., Nolan, P.L., Piner, B.G., Schneid, E., Sreekumar, P., and Thompson, D.J. 1993, *ApJ*, 407, L41
- Hughes, P.A., Aller, H.D., and Aller, M.F. 1985, *ApJ*, 298, 301
- Kniffen, D.A., Bertsch, D.L., Fichtel, C.E., Hartman, R.C., Hunter, S.D., Kanbach, G., Kwok, P.W., Lin, Y.C., Mattox, J.R., Mayer-Hasselwander, H.A., Michelson, P.F., von Montigny, C., Nolan, P.L., Pinkau, K., Schneid, E., Sreekumar, P., and Thompson, D.J. 1993, *ApJ*, 411, 133
- Krichbaum, T.P., Britzen, S., Standke, K.J., Witzel, A., and Zensus, J.A. 1995, in: *Quasars and AGN: High Resolution Radio Imaging*, ed. M. Cohen and K. Kellerman, proceedings of a Conference of the National Academy of Sciences, Irvine, CA, USA
- Levinson, A. 1996, *ApJ*, 459, 520
- Levinson, A., & Blandford, R. 1995, *ApJ*, 449, 86
- Lovelace, R.V.E., MacAuslan, J., & Burns, M.L. 1979, in *Particle Acceleration Mechanisms in Astrophysics*, ed. J. Arons, C. McKee, and C. Max (AIP Conf. Proc., 56, 399)
- Lovelace, R.V.E., & Romanova, M.M. 1995, in *Proceedings of Cygnus A Workshop*, C. Carelli & D. Harris, eds. (Cambridge: Cambridge Univ. Press)
- Lovelace, R.V.E., Newman, W.I., & Romanova, M.M. 1996, in preparation
- Lovelace, R.V.E., Romanova, M.M., & Newman, W.I. 1994, *ApJ*, 437, 136
- Lovelace, R.V.E., Wang, J.C.L., & Sulkanen, M.E. 1987, *ApJ*, 315, 504
- Mannheim, K., & Biermann, P.L. 1992, *A&A*, 253, L21
- Maraschi, L., Ghisellini, G., & Celotti, A. 1992, *ApJ*, 397, L5
- Marscher, A.P., & Bloom, S.D. 1992, in *The Compton Observatory Science Workshop*, (ed. C.R.Shader, N. Gehrels, and B.Dennis) NASA CP-3137, 346
- Mattox, J.R., Wagner, S.J., Malkan, M., McGlynn, T.A., Schachter, J.F., Grove, E., Johnson, N., Kurfess, J. 1996, *ApJ* (in press)
- Mattox, J.R., Bertsch, D.L., Chiang, J., Dingus, B.L., Fichtel, C.E., Hartman, R.C., Hunter, S.D., Kanbach, G., Kniffen, D.E., Kwok, P.W., Lin, Y.C., Mayer-Hassel-wander, H.A., Michelson, P.F., von Montigny, C., Nolan, P.L., Pinkau, K., Schneid, E., Sreekumar, P., and Thompson, D.J. 1993, *ApJ*, 410, 609
- Matveenko, L.I., Graham, D.A., Paulini-Toth, I.I.K., Sherwood, W.A., Bääth, L.B. & Kus, A. 1992, *Soviet Astronomy Letters*, 18, 979.
- Pacholczyk, A.G. 1970, *Radio Astrophysics* (Freeman: San Francisco) Ch. 3
- Pohl, M., Reich, W., Krichbaum, T.P., Standke, K., Britzen, S., Reuter, H.P., Reich, P., Schlickeiser, R., Fiedler, R.L., Waltman, E.B., Ghigo, F.D., & Johnston, K.J. 1995, *A & A*, in press
- Punch, M., et al. 1992, *Nature*, 358, 477
- Raga, A.C., Canto, J., Binette, L., & Calvet, N. 1990, *ApJ*, 364, 601
- Reich, W., Steppe, H., Schlickeiser, R., Reich, P., Pohl, M., Reuter, H.P., Kanbach, G., and Schonfelder, V. 1993, *Astron. & Astrophys.*, 273, 65
- Romanova, M.M., & Lovelace, R.V.E. 1992, *A&A*, 262, 26
- Sikora, M. 1994, *ApJ Suppl.*, 90, 923
- Sikora, M., Begelman, M.C., & Rees, M.J. 1994, *ApJ*, 421, 153
- Thompson, D.J., Bertsch, D.L., Dingus, B.L., Fichtel, C.E., Hartman, A.C., Hunter, S.D., Kanbach, G., Kniffen, D.A., Lin, Y.C., Mattox, J.R., Mayer-Hasselwander, H.A., Michelson, P.F., von Montigny, C., Nolan, P.L., Schneid, E.J., & Sreekumar, P. 1993, *ApJ*, 415, L13
- von Montigny, C., Bertsch, D.L., Chiang, J., Dingus, B.L., Esposito, J.A., Fichtel, C.E., Fierro, J.M., Hartman, R.C., Hunter, S.D., Kanbach, G., Kniffen, D.A., Lin, Y.C., Mattox, J.R., Mayer-Hasselwander, H.A., Michelson, P.F., Nolan, P.L., Radecke, H.D., Schneid, E., Thompson, D.J., & Willis, T. 1995, *ApJ*, 440, 525

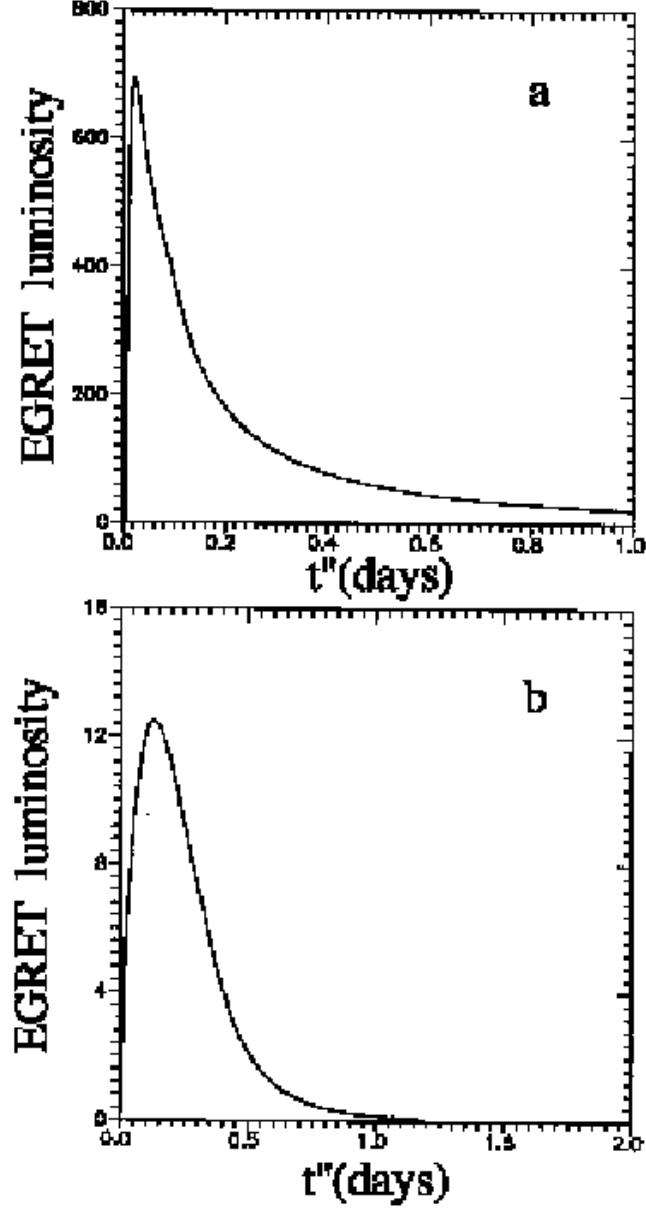


FIG. 9.— Typical light curves of apparent luminosity in the EGRET band in units of 10^{47} erg/s as measured by distant observer. In case (a), $f_{li}^o = 10$, and the light curve is determined by SSC processes. In case (b), $f_{li}^o = 20$, and the light curve is determined by the inverse-Compton process.

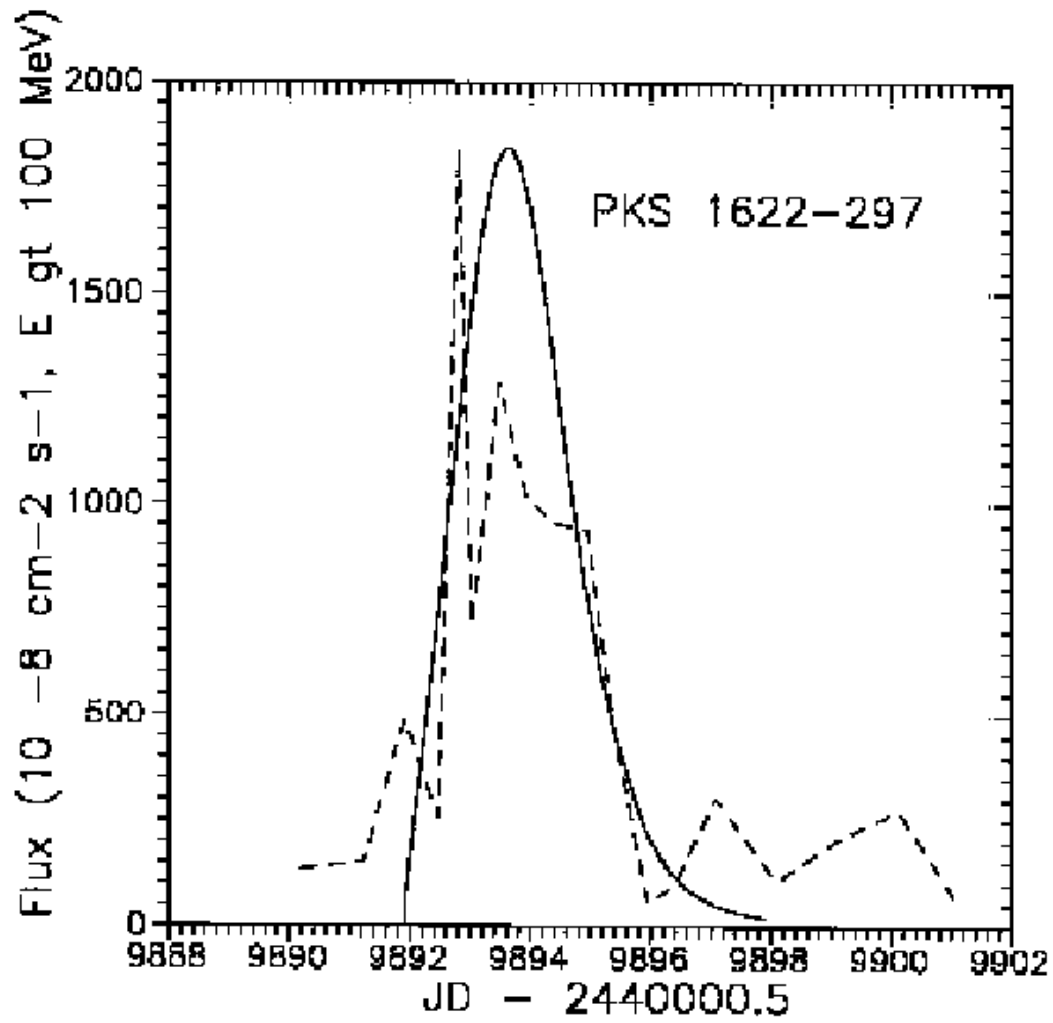


FIG. 10.— Comparison of the EGRET light curve of PKS 1622-297 (the dashed curve) (Mattox et al. 1996) with the calculated ‘Compton type’ light curve (solid curve).